IOP Publishing Journal of Physics A: Mathematical and Theoretical
J. Phys. A: Math. Theor. **48** (2015) 015101 (22pp) doi:10.1088/1751-8113/48/1/015101

Vehicular headways on signalized intersections: theory, models, and reality

Milan Krbálek and Jiří Šleis

Faculty of Nuclear Sciences and Physical Engineering, Czech Technical University in Prague, Prague, Czech Republic

E-mail: milan.krbalek@fjfi.cvut.cz

Received 1 April 2014, revised 9 October 2014
Accepted for publication 10 October 2014
Published 2 December 2014

Abstract

We discuss statistical properties of vehicular headways measured on signalized crossroads. On the basis of mathematical approaches, we formulate theoretical and empirically inspired criteria for the acceptability of theoretical headway distributions. Sequentially, the multifarious families of statistical distributions (commonly used to fit real-road headway statistics) are confronted with these criteria, and with original empirical time clearances gauged among neighboring vehicles leaving signal-controlled crossroads after a green signal appears. Using three different numerical schemes, we demonstrate that an arrangement of vehicles on an intersection is a consequence of the general stochastic nature of queueing systems, rather than a consequence of traffic rules, driver estimation processes, or decision-making procedures.

Keywords: microstructure of vehicular streams, analytically soluble models, signalized intersection models
PACS numbers: 05.40.-a, 89.40.-a, 47.70.Nd

(Some figures may appear in colour only in the online journal)

1. Introduction

Because of the empirical background, modeling of spatial positions of vehicles in the vicinity of signalized intersections continually attracts interest from researchers. As can be understood, the detection of statistical distributions of spatial/time headways among vehicles may lead to a more accurate determination of intersection capacities, which finally results in economic profit. Indeed, the importance of the topic can be inferred from the very frequent recent appearance of scientific papers dealing with intersection analyses. However, a majority of those works focus on macrodescription (for example, [1–4]) or (if concentrating on

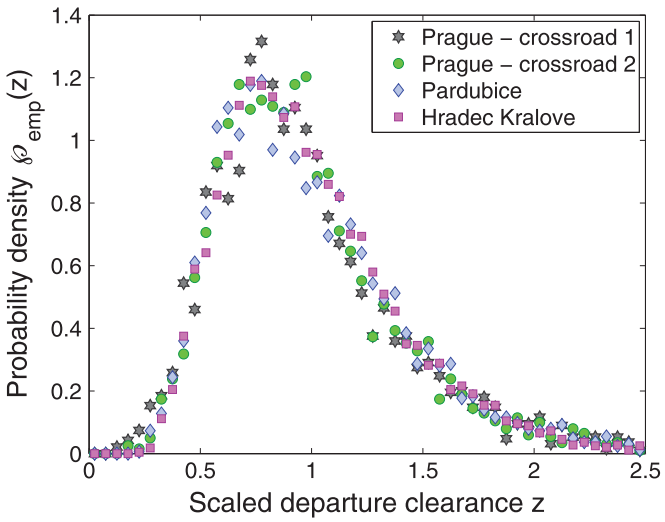

Figure 1. The empirical histogram of departure clearances. The constituent signs represent the statistical frequency of scaled net time gaps among neighboring cars leaving the intersections located as indicated in the legend.

microstructure) on average values of traffic microquantities (for example, [5–8]). In the past few years many studies investigating detailed statistical distributions of vehicular headways (spatial or time) between neighboring cars arising close to the stop line have been published. Some of them focus on the distribution of departure time intervals ([9–12]), and others on the distribution of spatial gaps between cars waiting for a green signal ([13, 14]).

In this article we intend to analyze a larger amount of original individual data gauged on various crossroads (located in the Czech cities Praha, Pardubice, and Hradec Králové) and to introduce suitable theoretical predictions for relevant probability densities of vehicular microquantities. Moreover, our aim is to create numerical representations of crossroad models leading to statistically consistent distributions. Finally, the analytical clearance distributions presented will be confronted with theoretical criteria derived from mutual vehicular interactions of short/middle-range nature. In the last part of the work, we will try to provide insight into the nature of the distributions examined.

A note: To prevent any misinterpretation, we remark that the respective descriptions for ranges of interactions (short/middle/long ranges) reflect how many neighboring elements (agents, particles, vehicles) interact with a chosen element. If a movement of the chosen agent is influenced by an immediately neighboring agent only, we will call such an interaction a short-ranged one. If there exist interactions among all agents in a system, this is referred to as a long-ranged case. Other interaction types are then classified as middle-ranged ones.

2. Empirical departure clearance statistics

The vehicular data analyzed in this work (see figure 1) were gauged on multi-lane intersections located in the centers of the Czech cities Praha (Prague), Pardubice and Hradec Králové. All the test intersections are constituents of an extensive network of roads and crossroads inside the internal metropolis and are therefore strongly saturated. In all cases the time interval between two green signals (on one crossroad) is short, which means that some

Table 1. Evaluation of data records before the scaling procedure is carried out.

Number	Location	Sample size	Mean clearance	Variance
1	Prague—crossroad 1	3785	1.6237 *s*	0.6649 s^2
2	Prague—crossroad 2	4022	1.5226 *s*	0.5023 s^2
3	Pardubice	3279	1.6110 *s*	0.4997 s^2
4	Hradec Králové	8795	1.5820 *s*	0.4185 s^2

cars are not able to reach the threshold of the following intersection during one green phase and therefore have to wait for another green light. This finally leads to a substantial decrease in average speed for cars moving among crossroads, i.e. one can observe here the effects detectable ordinarily in congested traffic regimes (see [15, 16]).

The traffic measurement has been organized as follows. The spontaneous traffic flow near the chosen intersection (see table 1) has been controlled by traffic lights in a usual mode. No external intervention has been applied. The gauging procedure (i.e. the measurement of the departure times $\tau_k^{(\mathrm{in})}$ and $\tau_k^{(\mathrm{out})}$—see the mathematical notation below) started at the moment of replacing the red signal by the green one and finished immediately after another red signal. We add that all analyzed traffic quantities have been measured only at intersections where other cars (moving in different lanes or in different arms) do not influence the gauged cars.

Thus, let the symbols $\tau_k^{(\mathrm{in})}$ and $\tau_k^{(\mathrm{out})}$ indicate the times at which the front/back bumpers of the kth car ($k = 0, 1, 2, \ldots, N$) have intersected a reference line (the stop line, typically) at the chosen intersection threshold. Then the *time clearance* between succeeding cars is defined as

$$t_k := \tau_k^{(\mathrm{in})} - \tau_{k-1}^{(\mathrm{out})} \quad (k = 1, 2, \ldots, N). \tag{1}$$

The fundamental quantity analyzed in our article is $z_k = t_k/\bar{t}$ for $k = 2,\ldots,N$, where $\bar{t} = \sum_{k=2}^{N} t_k \big/ (N-1)$, and it is referred to as the *scaled time clearance*. Note that the time gap between the first vehicle and the second vehicle has been discarded from the analysis. As shown in [9, 11, 12], the gap t_1 is longer than the other gaps. This is essentially due to the basic kinematic effect of a limited acceleration (see [12]). The empirical probability density $\wp_{\mathrm{emp}}(z)$ is then called the *(scaled) time clearance distribution*. To eliminate an unwelcome dependence of empirical distributions on the binning (quantization of the detected data into given smaller intervals—bins), one can define the integrated probability density (cumulative distribution function)

$$P_{\mathrm{emp}}(z) = \int_{-\infty}^{z} \wp_{\mathrm{emp}}(y)\mathrm{d}y. \tag{2}$$

The general quantitative results of a preliminary statistical analysis of gauged traffic data are summarized in table 1, where it can be seen that the mean clearance is about 1.6 s (with a standard deviation approximately equal to 0.7 s). Here we remark that the quantity measured for the purposes of this article (net gap) is different from the quantity (gross headway) analyzed in the research paper [9].

3. Criteria for acceptability of analytical clearance distributions

Owing to the empirical background of the topic investigated in this research, the curves representing theoretical approximations of the intersection clearance distribution have to fulfill both mathematical and empirically inspired criteria. Whereas mathematical criteria are

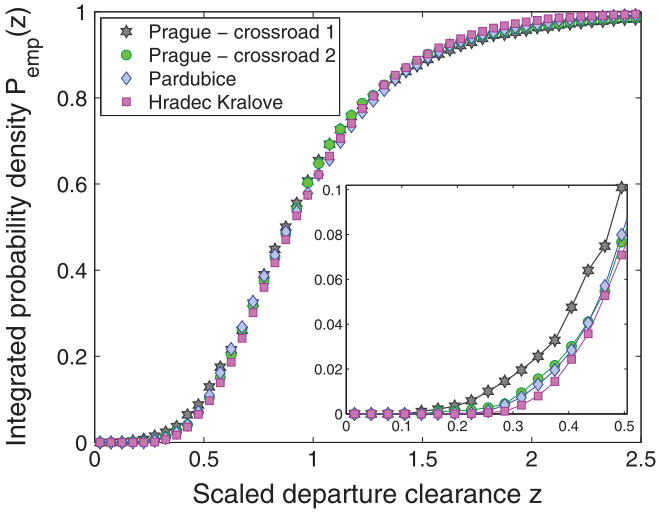

Figure 2. The cumulated histogram of departure time clearances. The constituent signs represent the cumulated probability density for scaled net time gaps detected among neighboring cars leaving the intersections located as indicated in the legend. The behavior of the cumulative distribution function near the origin is magnified in the inset.

deduced from exact theoretical definitions, empirical criteria reflect real features of traffic microstructure distributions (see for example [18, 25]). The measure for acceptability of theoretical curves can therefore be quantified using the number of fulfilled criteria.

First of all, we briefly summarize the mathematical criteria. If is intended that $\wp(z)$ will be declared a theoretical prediction for a time clearance distribution, it should fulfill the following theoretical criteria: **(T1)**—non-negativity: $\forall z \in \mathbb{R}$: $\wp(z) \geqslant 0$; **(T2)**—the support constraint: $\mathrm{supp}(\wp) = (0, \infty)$; **(T3)**—normalization: $\int_{\mathbb{R}} \wp(z)\mathrm{d}z = 1$; **(T4)**—scaling: $\int_{\mathbb{R}} z\,\wp(z)\mathrm{d}z = 1$; and finally **(T5)**—continuity: $\wp(z) \in \mathscr{C}(\mathbb{R}^+)$. We remark that the scaling criterion **T4** can be understood as optional.

In addition to these properties, some other requirements can be derived from recent knowledge about the microscopic structure of vehicular samples. As is apparent from many scientific sources (see [9, 10, 15, 17–25]), the spatial or temporal headway/clearance distributions (analyzed for congested traffic streams) show a heavy plateau located near the origin (see the figure 3 and the inset of the figure 2). That plateau is usually explained as a consequence of strong repulsions among closely occurring vehicles whose drivers make an effort to prevent a possible crash. In fact, such a phenomenon can be proven rigorously. Indeed, it is trivial to show that time–headway statistics have heavy left tails, because very small headways are unrealistic (due to the lengths of vehicles and the limited speed). In this case, there certainly exists a $\varepsilon > 0$ such that $\forall z \in (-\infty, \varepsilon)$: $\wp(z) = 0$. Since the clearance is in fact the headway reduced by the length of a car, the limit transition $\varepsilon \to 0_+$ corresponds to the headway $\to$ clearance transition. Accordingly, all clearance distributions measured in states with congested traffic should obey the condition

$$(\mathbf{E}1)\text{—the origin plateau:} \quad \forall\, q \in \mathbb{R}^+\colon \lim_{z \to 0_+} z^{-q}\wp(z) = 0. \tag{3}$$

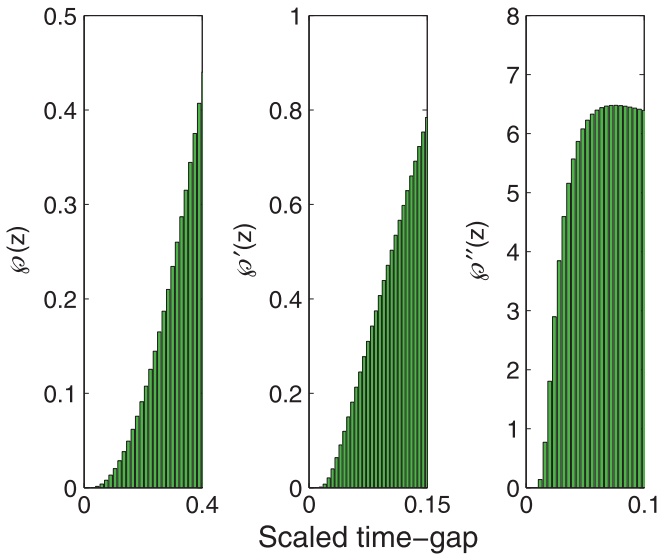

Figure 3. The graphical visualization of the origin plateau in the empirical clearance distributions. The bars display the smoothed probability density for short traffic clearances, and the first and second derivatives. The analyzed data (for traffic densities between 40 and 60 vehicles per kilometer) have been extracted from extensive data samples gauged on the two-lane freeway D1 (in the Czech Republic).

This condition is (for the locally smooth densities $\wp(z) \in \mathscr{C}^{\infty}(0, \delta)$) equivalent to the conditions $\dfrac{\mathrm{d}^m \wp}{\mathrm{d}z^m}(0_+) = 0$ for all $m \in N$. Unfortunately, $\wp(z)$ is not (as immediately follows from the preceding material) an analytical function, which therefore means that its Taylor expansion about the point zero is not allowed.

The second empirically inspired criterion is mathematically deduced from the conspicuous fact that all vehicular interactions are short/middle-ranged ones, i.e. the movements of two sufficiently outlying cars are not correlated (even in congested traffic). Such statistical ensembles used to be usually referred to as *quasi-Poissonian*. This terminology reflects the common knowledge that a system is qualified as *Poissonian (purely Poissonian)* if all associated subsystems are independent. In this case, the probability for the occurrence of several elements inside the fixed (space or time) region conforms to a Poissonian distribution. If the interactions among elements are restricted to several neighbors only, the Poissonian nature of adjacent elements is destroyed. In contrast, outlying elements still behave independently, which leads to the similarity between the distribution tail and that derived for Poissonian ensembles. Therefore, the tails of related headway distributions (for pure and quasi-Poissonian ensembles) show similar trends.

More formally: it is mathematically proven that all one-dimensional and purely Poissonian systems have the same probability density for scaled headways. Such a density reads $\wp(z) = \Theta(z)\mathrm{e}^{-z}$. Likewise, all one-dimensional and quasi-Poissonian ensembles necessarily produce headway distributions with tails of the same type. Such a special class of distributions is properly defined in the following definition.

Definition 4.1 A probability density $\wp(z)$ (with the associated distribution function) is called *balanced* if there exists $\omega > 0$ such that

$$\forall \varkappa > \omega: \quad \lim_{z\to+\infty} \wp(z)\mathrm{e}^{\varkappa z} = +\infty, \tag{4}$$

and

$$\forall \varkappa \in (0, \omega): \quad \lim_{z\to+\infty} \wp(z)\mathrm{e}^{\varkappa z} = 0. \tag{5}$$

The number ω is then called *the balancing index* and denoted by $\mathrm{inb}(\wp)$. The class of balanced distributions is denoted by $\mathscr{B}$.

As is evident, the family of balanced distributions and the family of heavy-tailed distributions (see [26, 27]) are disjoint. Thus, the intersection of $\mathscr{B}$ and the class $\mathscr{S}$ of subexponential distributions is empty. The same holds true also for the classes of fat-tailed and long-tailed distributions. Therefore the class $\mathscr{B}$ is a special subclass of light-tailed distributions. On the basis of an assumption that vehicular interactions are short/middle-ranged cases, the empirical net time gap distributions should also fulfill (see [28] as well) a final criterion:

$$(\mathbf{E}2)-\text{the balanced tail:} \quad \wp(z) \in \mathscr{B}. \tag{6}$$

4. Functional candidate time clearance distributions

According to the previous explorations of empirical clearances near signalized intersections [9–11, 13, 29, 30], the following noncomposite distribution models can be applied for describing real-road headway statistics: the *exponential distribution*, *Erlang distribution*, *Nakagami distribution* [31], *log-normal distribution*, and *generalized inverse Gaussian distribution* [32]. We emphasize that the exponential, Erlang, and generalized inverse Gaussian distributions represent (in contrast to the Nakagami and log-normal distributions) theoretically reasoned probability densities. Indeed, their forms have been derived as steady-state distributions for a local thermodynamic ensemble with short-ranged repulsions among the elements (see [33, 34]). After the scaling procedure, these distributions read as

$$\wp_{\mathrm{EXP}}(z) = \Theta(z)\mathrm{e}^{-z}, \tag{7}$$

$$\wp_{\mathrm{ERL}}(z) = \Theta(z)\frac{(\omega+1)^{\omega+1}}{\Gamma(\omega+1)}z^{\omega}\mathrm{e}^{-(\omega+1)z}, \tag{8}$$

$$\wp_{\mathrm{NAK}}(z) = 2\Theta(z)z^{2m-1}\frac{\Gamma^{2m}\left(m+\frac{1}{2}\right)}{\Gamma^{2m+1}(m)}\exp\left[-\frac{\Gamma^{2}\left(m+\frac{1}{2}\right)}{\Gamma^{2}(m)}z^{2}\right], \tag{9}$$

$$\wp_{\mathrm{LN}}(z) = \frac{\Theta(z)}{\sqrt{2\pi}\sigma z}\exp\left[-\frac{\left(\sigma^{2}+2\ln(z)\right)^{2}}{8\sigma^{2}}\right]. \tag{10}$$

Likewise, the additional probability density $\wp_{\mathrm{GIG}}(z) = A\exp[-\beta/z - Dz]$ (considered in the articles [13, 15, 22, 24, 33] and analyzed in the book [32]) requires proper normalization and scaling. Owing to the functional relation

$$\int_0^{\infty} \mathrm{e}^{-\frac{x^2}{4t}}\mathrm{e}^{-t}\,\mathrm{d}t = x\mathcal{K}_1(x), \tag{11}$$

where $\mathcal{K}_1(x)$ stands for the Macdonald function of the first order—a solution of the modified Bessel differential equation of the second kind (of order $\alpha \in \mathbb{N}$)

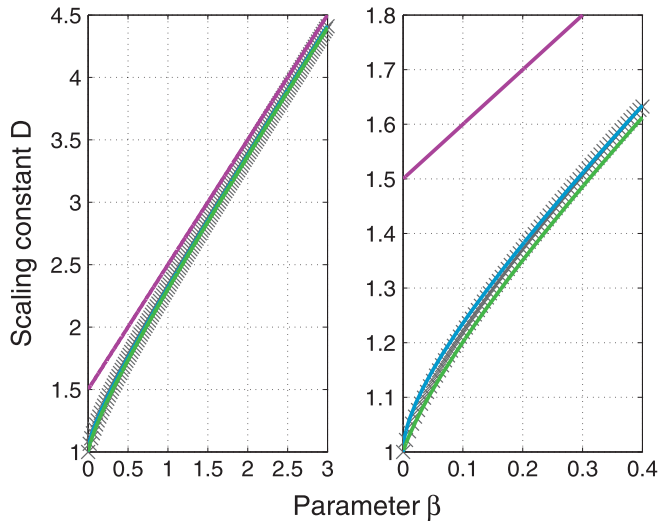

Figure 4. The calibration of the scaling constant $D = D(\beta)$ in the generalized inverse Gaussian distribution. The red, blue, and green curves represent the asymptotical dependence (17), phenomenological approximation (18), and analytical approximation (16), respectively. The crosses display numerical solutions of the scaling equality $\int_{\mathbb{R}} \wp_{\mathrm{GIG}}(z)\mathrm{d}z = \int_{\mathbb{R}} z\wp_{\mathrm{GIG}}(z)\mathrm{d}z$.

$x^2y'' + xy' - (x^2 + \alpha^2)y = 0$, one can derive the value of the normalization constant

$$A^{-1} = 2\sqrt{\frac{\beta}{D}}\,\mathcal{K}_1\Big(2\sqrt{\beta D}\Big). \tag{12}$$

Substituting $z(x) := x^\alpha \mathrm{e}^x \mathcal{K}_\alpha(x)$ into the original Bessel equation, we obtain the differential equation $xz'' - (2\alpha + 2x - 1)z' + (2\alpha - 1)z = 0$ which (together with the Cauchy's initial conditions $z(0) = z'(0) = (2\alpha - 2)\,!!$) provides a small-$x$ approximation:

$$\mathcal{K}_\alpha(x) \approx (2\alpha - 2)\,!!\left(1 + \frac{2x}{2\alpha - 1}\right)^{\alpha - 1/2}\frac{\mathrm{e}^{-x}}{x^\alpha} \tag{13}$$

that is more suitable than the well-known approximation $\mathcal{K}_\alpha(x) \approx \mathrm{e}^{-x}/x^\alpha$. Since the above-mentioned integrals **T3** and **T4** fulfill the differential equation

$$\int_0^\infty x\mathrm{e}^{-\frac{\nu^2}{x}}\mathrm{e}^{-\varkappa^2 x}\,\mathrm{d}x = -\frac{1}{2\varkappa}\frac{\partial}{\partial\varkappa}\int_0^\infty \mathrm{e}^{-\frac{\nu^2}{x}}\mathrm{e}^{-\varkappa^2 x}\,\mathrm{d}x, \tag{14}$$

the scaling condition (**T4**) can be reformulated (applying the approximation (13)) as the cubic equation

$$4\nu\varkappa^3 + \left(1 - 4\nu^2\right)\varkappa^2 - 4\nu\varkappa - 1 = 0. \tag{15}$$

Its real solution then provides a desired functional relation guaranteeing fulfillment of the scaling condition. Such a relation is of the form

$$D \approx \left(\frac{4\beta + w(\beta) + \frac{16\beta^2 + 40\beta + 1}{w(\beta)} - 1}{12\sqrt{\beta}} \right)^2, \tag{16}$$

where $w^3(\beta) = 4\left(16\beta^3 + 60\beta^2 + 3\sqrt{48\beta^3 + 132\beta^2 - 3\beta} + 39\beta \right) - 1$. Asymptotical features of the normalization dependence $D = D(\beta)$ may be quantified by the relations

$$\lim_{\beta \to 0_+} D(\beta) = 1, \quad D(\beta) \approx \beta + \frac{3}{2} (\beta \gg 1). \tag{17}$$

The accuracy of the previous approximate calculations is demonstrated in figure 4, where the numerically specified values D are confronted with the analytically and phenomenologically specified values. To conclude, one can briefly summarize by saying that the relation

$$D(\beta) \approx \beta + \frac{3 - \mathrm{e}^{-\sqrt{\beta}}}{2} \tag{18}$$

represents a sufficient approximation of the scaling constant in the generalized inverse Gaussian distribution, which means that the probability density

$$\wp_{\mathrm{GIG}}(z) = \frac{\sqrt{D}\ \Theta(z)}{2\sqrt{\beta}\,\mathcal{K}_1\left(2\sqrt{\beta D}\right)} \exp\left[-\frac{\beta}{z} - Dz \right], \quad D = \beta + \frac{3 - \mathrm{e}^{-\sqrt{\beta}}}{2} \tag{19}$$

completes the set of noncomposite probabilistic models convenient for the purposes of this work.

In table 2, we summarize the relevant properties of all above-mentioned distributions. As is apparent, the one and only probabilistic model fulfilling all the requisite criteria is the model derived as a steady-state solution for the thermal-like vehicular simulator presented in the articles [33] and [34]. The other distributions show at least one incompatibility with theoretical requirements. However, all suggested functions can be used for comparing with empirical clearance distributions gauged between neighboring vehicles leaving a chosen signal-controlled intersection. For these purposes we define the generalized statistical distance

$$\chi(\varepsilon) = \int_0^\infty |\wp(z;\, \varepsilon) - q(z)|^2\, z\mathrm{e}^{1-z}\, \mathrm{d}z \tag{20}$$

cumulating the weighted deviations between a theoretical one-parametric prediction $\wp(z;\, \varepsilon)$ and the empirical frequency $q(z)$. The optimal value of the estimated parameter $\hat{\varepsilon}$ can then be evaluated by minimizing the statistical distance (20), i.e.,

$$\hat{\varepsilon} = \mathrm{argmin}_{\varepsilon \in [0,\infty)} \int_0^\infty |\wp(z;\, \varepsilon) - q(z)|^2\, z\mathrm{e}^{1-z}\, \mathrm{d}z. \tag{21}$$

The tangible results of such procedures are tabularized in tables 3 and 4 where optimal values of the estimated parameters are summarized as well as minimum values of weighted statistical distances (20) specified for the above-mentioned optimal parameters. We remark that the weight factor $\phi(z) = z \exp[1 - z]$ has been chosen (a) to eliminate the influence of long clearances, (b) to suppress extremely short clearances, and finally (c) to increase the influence of clearances that are close to the mean value. In addition, $\mathrm{argmax}_{z \geqslant 0} \phi(z) = 1$ and $\phi(1) = 1$.

Table 2. Criteria of acceptability for various noncomposite probabilistic models.

Probability density	(**T1**)	(**T2**)	(**T3**)	(**T4**)	(**T5**)	(**E1**)	(**E2**)
$\wp_{\mathrm{EXP}}(z)$	Yes	Yes	Yes	Yes	Yes	No	Yes
$\wp_{\mathrm{ERL}}(z)$	Yes	Yes	Yes	Yes	Yes	No	Yes
$\wp_{\mathrm{NAK}}(z)$	Yes	Yes	Yes	Yes	Yes	No	No
$\wp_{\mathrm{LN}}(z)$	Yes	Yes	Yes	Yes	Yes	Yes	No
$\wp_{\mathrm{GIG}}(z)$	Yes	Yes	Yes	Yes	Yes	Yes	Yes

5. The rigidity of quasi-poissonian ensembles

Configurations of vehicles in the neighborhood of an intersection used to be typically analyzed, as discussed in the previous sections, by means of statistical instruments applied to gaps or time intervals between departures of succeeding cars (see [9–11, 13, 14]). Although recent researchers have proposed certain candidate distance/time clearance distributions, a way to evaluate such probabilistic models is still lacking. Concurrently, a felicitous evaluation scheme has become available in random matrix theory [35]. Here a mathematical quantity (called the *spectral rigidity* or *number variance*) is defined. This quantity surveys a structure of eigenvalue clusters in ensembles of random matrices. The notable advantages of such an approach are as follows:

1. The spectral rigidity quantifies (unlike the clearance distribution) an arrangement of larger clusters of particles/cars/eigenvalues.
2. The functional formula for the rigidity is directly connected to the clearance distribution, which could yield an interesting alternative for verifying newly suggested probabilistic predictions against empirical data.
3. The geometric shapes of the rigidity curves are extremely simple.
4. The statistical analysis of spectral rigidity for data files is undemanding.
5. A slight change of a parameter in the clearance distribution leads to a marked change in the graph of the rigidity, which demonstrates the strong sensitivity of rigidity testing. On the other hand, the disadvantage of rigidity tests is a sensitivity to correlations among headways. Two distributions with the same headway (with different levels of headway correlations) can produce different slopes in the graph of the rigidity. This effect is noticeably visible in figures 2 and 5 (compare the circles and diamonds in the two figures). For these reasons, a rigidity test always has to be accompanied by a statistical analysis of headways/clearances.

On reformulation within the bounds of traffic theory, the rigidity coincides with the following interpretation. Consider a set $\{z_i \in \mathbb{R}^+ \colon 1 \ldots N\}$ of scaled time clearances between each pair of subsequent cars. Since we suppose that the mean time gap taken over the complete set is rescaled to 1, it holds that $\sum_{i=1}^{N} z_i = N$. After dividing the time interval $[0, N)$ into subintervals $[(k-1)T, kT)$ of length T, one can define a new random variable $n_k(T)$ representing the number of cars whose departure times belong to the kth subinterval. The average value $\bar{n}(T)$ taken over all possible subintervals is therefore

Table 3. Optimal values of parameters for various one-parametric probabilistic models.

Location	$\wp_{\mathrm{ERL}}(z)$	$\wp_{\mathrm{NAK}}(z)$	$\wp_{\mathrm{LN}}(z)$	$\wp_{\mathrm{GIG}}(z)$
Prague—cross-road 1	$\hat{\omega} = 4.8350$	$\hat{m} = 1.6619$	$\hat{\sigma} = 0.41931$	$\hat{\beta} = 2.0507$
Prague—cross-road 2	$\hat{\omega} = 5.3017$	$\hat{m} = 1.7939$	$\hat{\sigma} = 0.40551$	$\hat{\beta} = 2.2489$
Pardubice	$\hat{\omega} = 4.6100$	$\hat{m} = 1.6116$	$\hat{\sigma} = 0.43015$	$\hat{\beta} = 1.9172$
Hradec Králové	$\hat{\omega} = 5.4536$	$\hat{m} = 1.8281$	$\hat{\sigma} = 0.39985$	$\hat{\beta} = 2.3195$

Table 4. Statistical distances (20) for various one-parametric probabilistic models.

Location	$\chi_{\mathrm{EXP}}(z)$	$\chi_{\mathrm{ERL}}(z)$	$\chi_{\mathrm{NAK}}(z)$	$\chi_{\mathrm{LN}}(z)$	$\chi_{\mathrm{GIG}}(z)$
Prague—crossroad 1	5.9368	0.43766	0.83113	0.24556	0.27659
Prague—crossroad 2	6.5770	0.35958	0.75371	0.14868	0.17275
Pardubice	5.9281	0.28204	0.61882	0.11643	0.11985
Hradec Králové	6.5628	0.13128	0.42344	0.02901	0.02859

$$\overline{n}(T) = \frac{1}{\lfloor N/T \rfloor} \sum_{k=1}^{\lfloor N/T \rfloor} n_k(T) = T, \tag{22}$$

where the integer part $\lfloor N/T \rfloor$ stands for the number of all subintervals $[(k-1)T, kT)$ included in the entire interval $[0, N)$. We suppose, for convenience, that N/T is an integer. The *time rigidity* $\Delta(T)$ is then defined as

$$\Delta(T) = \frac{T}{N} \sum_{k=1}^{N/T} \big(n_k(T) - T\big)^2. \tag{23}$$

Provided that all variables are independent (which is not the general case), the formula (23) represents the statistical variance of the number of vehicles passing a given fixed point (a threshold of the intersection, typically) during the time interval T. In view of the fact that the expected value $\mathrm{E}(n(T))$ and the average value $\overline{n}(T)$ can differ (for systems of dependent random variables), we will not use the term 'variance'. It is self-evident that for ensembles of equidistantly spaced elements, the statistical rigidity reads

$$\Delta_{\mathrm{EQD}}(T) = (T - \lfloor T \rfloor)(\lfloor T \rfloor + 1 - T). \tag{24}$$

Denoting as $\wp_\ell(z)$ the distribution of net time gaps between $\ell + 2$ cars (i.e. $\wp_0(z) = \wp(z)$ is the standard clearance distribution), one can define the *cluster function*

$$R(z) = \sum_{\ell=0}^{\infty} \wp_\ell(z), \tag{25}$$

which is closely related to the random variable $n(T)$—the number of particles departing from a chosen location during the time interval T. Indeed, the probability $\mathbb{P}[n(T) = \ell]$ that exactly ℓ cars pass the stop line during an arbitrary time interval of length T can be expressed in terms of multiclearance distributions $\wp_\ell(z)$ as

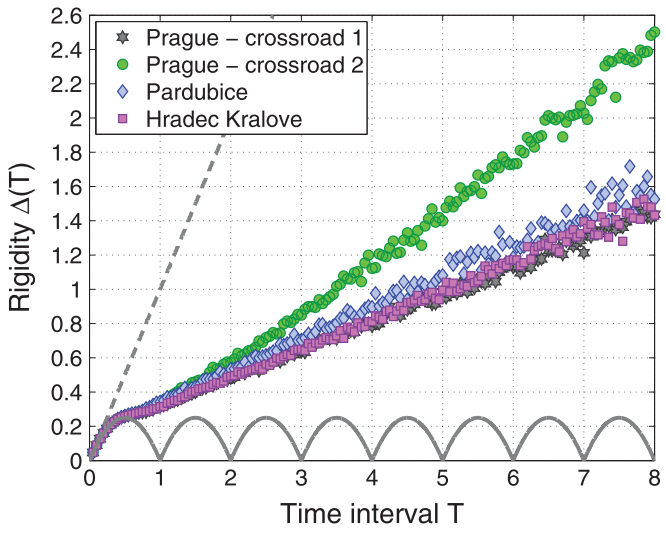

Figure 5. The rigidity of empirical traffic data. The signs represent the statistical rigidity $\Delta(T)$ analyzed for clusters of cars leaving the intersections located according to the legend. The dashed line and wavy line symbolize the statistical rigidities calculated for ensembles of uncorrelated (34) and equidistantly spaced (24) particles, respectively.

$$\mathbb{P}[n(T)=0]=1-\int_0^T \wp_0(z)\mathrm{d}z,\ \mathbb{P}[n(T)=\ell]=\int_0^T \big(\wp_{\ell-1}(z)-\wp_\ell(z)\big)\mathrm{d}z. \tag{26}$$

Hence the average value of $n(T)$ is

$$\mathrm{E}(n(T))=\sum_{\ell=0}^{\infty}\ell\,\mathbb{P}[n(T)=\ell]=\int_0^T R(z)\mathrm{d}z. \tag{27}$$

Furthermore,

$$\mathrm{E}\Big(n^2(T)\Big)=\sum_{\ell=0}^{\infty}\ell^2\mathbb{P}[n(T)=\ell]=\int_0^T (2S(z)-R(z))\mathrm{d}z, \tag{28}$$

where $S(z)=\sum_{\ell=0}^{\infty}\ell\wp_\ell(z)$. Since $R(z)\star R(z)=S(z)-R(z)$ (as follows from rules derived for functional convolutions), the rigidity can be computed via

$$\begin{aligned}\Delta(T)&=\sum_{\ell=0}^{\infty}(\ell-T)^2\mathbb{P}[n(T)=\ell]\\&=2\int_0^T (R\star R)(z)\mathrm{d}z+\Big(1-2\,T\Big)\int_0^T R(z)\mathrm{d}z+T^2.\end{aligned} \tag{29}$$

Assuming an approximate equality $\mathrm{E}(n(T))\approx\overline{n}(T)$, i.e. $\int_0^T R(z)\mathrm{d}z\approx T$, and using the convolution property $\int_0^T (R\star R)(z)\mathrm{d}z=R(T)\star\int_0^T R(z)\mathrm{d}z$, we obtain the closing formula for the statistical rigidity:

$$\Delta(T)\approx T-2\int_0^T (T-z)(1-R(z))\mathrm{d}z. \tag{30}$$

According to articles [24, 36], the Laplace image of cluster functions of quasi-Poissonian ensembles analyzed in our paper, i.e. ensembles with balanced tails (see the definition 4.1),

reads

$$\mathscr{L}\big[R_{\mathrm{EXP}}\big](p) = \frac{1}{p}, \tag{31}$$

$$\mathscr{L}\big[R_{\mathrm{ERL}}\big](p) = \frac{1}{\left(1+\frac{p}{\omega+1}\right)^{\omega+1}-1} = \frac{1}{p} - \frac{\omega}{2(\omega+1)} + \frac{p\omega(\omega+2)}{12(\omega+1)^2} + \mathcal{O}\left(p^2\right), \tag{32}$$

$$\begin{aligned}\mathscr{L}\big[R_{\mathrm{GIG}}\big](p) &\approx \left(\frac{D+p}{D}\,\frac{\mathrm{e}^{2\sqrt{(D+p)\beta}}}{\mathrm{e}^{2\sqrt{D\beta}}} - 1\right)^{-1} \\ &\approx \frac{1}{p} - \frac{2D\beta+3\sqrt{D\beta}}{4\left(1+\sqrt{D\beta}\right)^2} + p\frac{6\sqrt{D\beta}+D\beta\left(21+4D\beta+16\sqrt{D\beta}\right)}{48D\left(1+2\sqrt{D\beta}\right)^3} + \mathcal{O}\left(p^2\right).\end{aligned} \tag{33}$$

As the formula (30) can be rewritten in the form

$$\Delta(T) \approx T - 2\Theta(T)T\star\Theta(T) + 2\Theta(T)T\star R(T),$$

the linear trend $\Delta(T) \approx \lambda T + \mu$ near infinity may be revealed (after applying the Laplace transformation) with the help of

$$\lambda p + \mu p^2 \approx p - 2 + 2p\mathscr{L}[R](p).$$

Taylor's expansion for the function $p\mathscr{L}[R](p)$ then finalizes the process of rigidity linearization. Hence the linear tails of the adjoint rigidities are given by

$$\Delta_{\mathrm{EXP}}(T) = T, \tag{34}$$

$$\Delta_{\mathrm{ERL}}(T) \approx \frac{T}{\omega+1} + \frac{\omega(\omega+2)}{6(\omega+1)^2}, \tag{35}$$

$$\Delta_{\mathrm{GIG}}(T) \approx \frac{2+\sqrt{D\beta}}{2D\left(1+\sqrt{D\beta}\right)}T + \frac{6\sqrt{D\beta}+D\beta\left(21+4D\beta+16\sqrt{D\beta}\right)}{24\left(1+2\sqrt{D\beta}\right)^4}. \tag{36}$$

As is well known from random matrix theory, the linear asymptote $\Delta(T) \approx \lambda T + \mu$ (characterizing the course of the rigidity near infinity) demonstrates the short-ranged nature of component interactions, which is in consonance with the general meaning of the driver interactions. In fact, on investigating the statistical rigidity in vehicular samples, one can detect typical linear tails in all data samples examined (see figure 5). Moreover, as expected, the rigidities of all probabilistic models presented show linear tails, and for that reason one can compare the related slopes λ with those obtained by analyzing empirical data. The quantitative outcome of such a comparison is summarized in table 5, where we show the values of the rigidity slopes λ obtained for the parameters (and models) summarized in table 3. For completeness, we add that the statistical rigidities for exponential, Erlang, and GIG distributions have been acquired analytically, whereas the Nakagami and log-normal rigidities has been observed numerically.

6. Assessment of suggested probabilistic models

In the previous sections we have suggested and evaluated five probability distributions that are broadly accepted as analytical vehicular headway distribution candidates. As

Table 5. The slope λ in the theoretical and empirical rigidities.

Location	$\lambda_{\text{intersection}}$	λ_{EXP}	λ_{ERL}	λ_{NAK}	λ_{LN}	λ_{GIG}
Prague—crossroad 1	0.1625	1.0000	0.1821	0.1706	0.1930	0.1873
Prague—crossroad 2	0.3048	1.0000	0.1617	0.1474	0.1732	0.1738
Pardubice	0.1815	1.0000	0.1816	0.1720	0.2074	0.1961
Hradec Králové	0.1691	1.0000	0.1573	0.1516	0.1658	0.1692

demonstrated by the previous quantitative and qualitative evaluations, the choice of candidate seems to be effortless. However, the selected evaluation criteria give stronger preference to the log-normal and generalized inverse Gaussian models, because both of them fit the empirical histograms in such a way that the statistical distance (20) becomes rapidly smaller than that evaluated for exponential, Erlang, and Nakagami models. Furthermore, the associated rigidities (empirical and log-normal/GIG) are also in a plausible correspondence. Taking into consideration the theoretical and empirically inspired criteria (***T*1**–***T*5** and ***E*1**–***E*2**), we can convincingly conclude that the best theoretical predictions for vehicular departure times have been achieved by means of the probability density (19). Finally, we recall that a great advantage of the GIG model is the fact that the proposed density is of socio-physical essence. Indeed, the distribution (19) has been identified in the articles [22, 28, 33, 34] as a steady-state distribution of a certain socio-physical traffic model. In addition to that, the book [32] points out that the probability density (19) characterizes a distribution of times between events in some renewal processes. These findings support the final result of our evaluation procedure.

7. Leave-the-intersection models: the GCF scheme

In the following three sections we will propose three traffic models, aiming to explain the core of departure clearance distributions, and in particular to reproduce the observed vehicular gap distributions on signal-controlled crossroads. The first of them is based on the car-following principles discussed in [9, 11, 20, 39, 40] and on the theory of the so-called Galton board (see [37]). Such a model will be referred to as a *GCF model*. The parameters of the model and brief explanations of them are summarized in table 6.

Consider N identical dimensionless particles located at the time $t = 0$ in sequentially organized locations $x_N < x_{N-1} < \ldots < x_2 < x_1 < 0$. Here the origin $x = 0$ represents an intersection threshold. For brevity of the following notation, we denote the space headway in front of the ℓth particle as r_ℓ, i.e., $r_\ell := x_{\ell-1} - x_\ell$. At the beginning of each realization of the GCF algorithm, the initial velocities $v_1, v_2, \ldots, v_N \geqslant 0$ of all particles are set to zero and the initial positions are randomized according to the selected distribution. Copying the approach in [9], we introduce a Boolean variable F_ℓ signaling whether the ℓth vehicle is in the starting-up mode ($\mathrm{F}_\ell = 1$) or not.

The simulating scheme is divided into three main modes: *(1) the stopped mode*, *(2) the starting-up mode*, and *(3) the moving mode*. The latter is composed of three submodels: *(3a) the free-driving submode*, *(3b) the braking submode*, and *(3c) the car-following submode*. Dynamical rules for the transition of an ensemble from an original state (at the time t) to an

Table 6. Parameters of the *GCF model*.

Nomenclature	General extent	Option	Description
w_{start}	$\in[2, 3]$ m s^{-1}	2.7 m s^{-1}	Velocity delimiting the starting mode
w_{max}	$\in[10, 20]$ m s^{-1}	16 m s^{-1}	Maximum velocity
a_{start}	$\in[2, 5]$ m s^{-2}	2 m s^{-2}	Run-up acceleration
a_{plus}	$>a_{\text{start}}$	4.4 m s^{-2}	Maximum free-driving acceleration
a_{minus}	$\approx 2a_{\text{plus}}$	7 m s^{-2}	Maximum braking deceleration
g_{start}	$\in[1, 3]$ m	2.2 m	Minimum distance required for moving off
g_{min}	$\in(0, 1]$ m	0.5 m	Minimum safety clearance
g_{max}	>10 m	15 m	Distance limit for free-driving mode
H	$\in[1, 10]$ s	8 s	Deceleration time
p	$\in(0, 1)$	0.38	Random-deceleration rate
ϑ	$\in(0, 1)$	0.8	Decelerating factor

updated state (at the time $t + \mathrm{T}$, where T denotes the size of the simulation time step) are then strictly derived from the above-mentioned modes.

7.1. The stopped mode

The entering condition for this mode is $v_\ell(t) = 0$. The ℓth vehicle will enter the starting-up mode at the time $t + \mathrm{T}$ (and $\mathrm{F}_\ell(t + \mathrm{T})$ will be set to 1) if $r_\ell(t) > g_{\text{start}}$; otherwise the vehicle will continue in the actual mode.

7.2. The starting-up mode

If $\mathrm{F}_\ell(t) = 1$, the move of the ℓth vehicle will be regulated by the starting-up rule. If $v_\ell(t) \geqslant w_{\text{start}}$, then the ℓth vehicle will enter the moving mode at the time $t + \mathrm{T}$ and $\mathrm{F}_\ell(t + \mathrm{T})$ will be set to 0. In contrast, if $v_\ell(t) < w_{\text{start}}$, then $\mathrm{F}_\ell(t + \mathrm{T}) := 0$ and

$$v_\ell(t + \mathrm{T}) := \Theta\big(r_\ell(t) - g_{\text{min}}\big)\big(v_\ell(t) + a_{\text{start}}\mathrm{T}\big), \tag{37}$$

where $\Theta(x)$ is the Heaviside step-function.

7.3. The free-driving submode

If and only if $v_\ell(t) \geqslant w_{\text{start}}$ and the distance headway $r_\ell(t)$ becomes larger than the distance limit g_{max}, then the vehicle enters the free-driving submode. Then

$$v_\ell(t + \mathrm{T}) := \min\left\{v_\ell(t) + a_{\text{plus}}\mathrm{T},\, w_{\text{max}}\right\}. \tag{38}$$

7.4. The braking submode

If and only if $v_\ell(t) \geqslant w_{\text{start}}$, $r_\ell(t) < g_{\text{max}}$, and

$$v_\ell(t) - v_{\ell-1}(t) > \frac{r_\ell(t) - g_{\text{min}}}{H}, \tag{39}$$

there is a risk of collision. Therefore the velocity must be reduced as follows:

$$v_\ell(t+\mathrm{T}) := \max\left\{v_\ell(t) - a_{\mathrm{minus}}\mathrm{T},\, 0\right\}. \tag{40}$$

7.5. The car-following submode

If and only if $v_\ell(t) \geqslant w_{\mathrm{start}}$, $r_\ell(t) < g_{\max}$, and

$$v_\ell(t) - v_{\ell-1}(t) \leqslant \frac{r_\ell(t) - g_{\min}}{H}, \tag{41}$$

the driver carefully adapts his/her maneuvering to a previous car. Specifically, the Galton-inspired stochastic update rule for the car-following process (see [37, 38]) is introduced:

$$v_\ell\left(t+\frac{\mathrm{T}}{2}\right) := \begin{cases} \dfrac{r_\ell(t)}{r_\ell(t-\mathrm{T})}\vartheta v_\ell(t) & \ldots \text{ with probability } \quad p, \\ \max\left\{\dfrac{r_\ell(t)}{r_\ell(t-\mathrm{T})}\dfrac{v_\ell(t)}{\vartheta},\, w_{\mathrm{start}}\right\} & \ldots \text{ with probability } \quad 1-p, \end{cases} \tag{42}$$

$$v_\ell(t+\mathrm{T}) := \min\left\{v_\ell(t) + a_{\mathrm{plus}}\mathrm{T};\, v_\ell\left(t+\frac{\mathrm{T}}{2}\right)\right\}. \tag{43}$$

7.6. The forward-ordered update

Finally, the positions of particles are sequentially updated (in forwardly directed order) as follows:

$$x_\ell(t+\mathrm{T}) = x_\ell(t) + \mathrm{T}\cdot v_\ell(t+\mathrm{T}). \tag{44}$$

The above-mentioned update rules, defining the forward-ordered sequential dynamics of the system, have been repeatedly applied to actual configurations until the last car has intersected the stop line. Denoting the time at which the ℓth car has reached the measuring point $x = 0$ as τ_ℓ, one can intuitively define the scaled clearances as

$$z_\ell = (N-1)\frac{\tau_\ell - \tau_{\ell-1}}{\tau_N - \tau_1} \quad (\ell \in \{2, 3, \ldots, N\}). \tag{45}$$

These normalized time gaps are independent of the time step size T and represent the main quantities investigated in this paper. Therefore, after repeated realizations of the GCF algorithm (with the initialization $N = 12$ and $\mathrm{T} = 0.3$), we can proceed to an expected statistical evaluation. The graphical outputs of such an evaluation are visualized in figure 6. Here one can compare the clearance distributions between empirical and GCF data (10 000 clearances), as well as the respective statistical rigidities. Although certain similarities can be found there, deviations between the model and reality for the traffic are significant.

8. Leave-the-intersection models: the PLCF scheme

The second design for an intersection model (here called the *phenomenological car-following model*) is based on the work [41] and the more recent results published in [18, 25]. Like in the previous section, we firstly introduce all parameters of the model suggested (see table 7).

Our PLCF modification eliminates a slight illogicality in the original conception presented in [41]—namely, an occurrence of two vehicles moving with the same velocities and

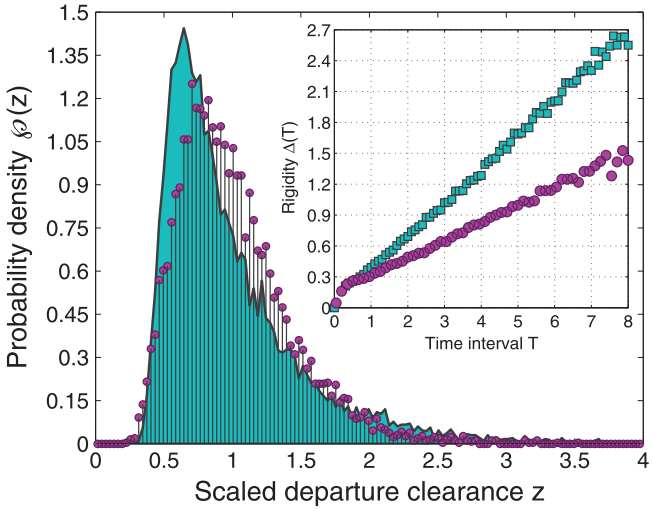

Figure 6. Clearance distributions and statistical rigidities for the GCF model. The main plot compares the clearance distributions, between real-road data (Hradec Králové—circles) and the Galton-inspired car-following model (the area plot) presented in the text. The comparison between the statistical rigidities (for the same data ensembles) is presented in the inset.

with zero clearance (i.e., cars moving like connected objects) is in fact extremely improbable. Therefore, we eliminate such a circumstance by introducing a minimum (i.e., safety) bumper-to-bumper distance $g_{\min}$ that is randomly chosen from the exponential distribution Exp (ε) with parameter $\varepsilon > 0$. Now, the simulation scheme replicates the general strategy of the GCF model. Specifically, we consider N particles placed in locations $x_N < x_{N-1} < \ldots < x_2 < x_1 < 0$ and moving with velocities $v_1, v_2, \ldots, v_N \geqslant 0$. Again, bumper-to-bumper distances are denoted by r_ℓ. Furthermore, we define the so-called *safe velocity*

$$v_{\mathrm{safe}_\ell}(t) = v_{\ell-1}(t) + \frac{r_\ell(t) - g_{\min_\ell} - \mathrm{T}\cdot v_{\ell-1}(t)}{\frac{v_\ell(t)+v_{\ell-1}(t)}{2a_{\mathrm{minus}}} + \mathrm{T}}, \tag{46}$$

whose rigorous form is derived (see [41]) by requiring a collision-free condition and limitedness of vehicular accelerations. By means of the safe-velocity approach, we can express the *desired velocity* as

$$v_{\mathrm{des}_\ell}(t) = \min\left\{w_{\max};\, v_{\mathrm{safe}_\ell}(t);\, v_\ell(t) + \mathrm{T}\cdot a_{\mathrm{plus}}\right\}. \tag{47}$$

Then the randomly perturbed velocity (influenced by the phenomenological coefficient θ suppressing the velocity variance in the ensemble) satisfies the equation

$$v_\ell(t+\mathrm{T}) = \max\left\{0;\, \mathrm{Uni}\Big(v_{\mathrm{des}_\ell}(t) - \theta\cdot\mathrm{T}\cdot a_{\mathrm{minus}}\Big),\, v_{\mathrm{des}_\ell}(t)\Big)\right\}, \tag{48}$$

where the symbol $\mathrm{Uni}(a, b)$ corresponds to the continuous uniform distribution on the interval (a, b). Finally, the positions of particles are standardly updated (in the forwardly directed order, again) according to

Table 7. Parameters of the *PLCF model*.

Nomenclature	General extent	Option	Description
$w_{\max}$	$\in[10, 20]$ m s^{-1}	14 m s^{-1}	Maximum allowable velocity
a_{plus}	$\in[3, 5]$ m s^{-2}	4.35 m s^{-2}	Maximum free-driving acceleration
a_{minus}	$\in[4, 8]$ m s^{-2}	7 m s^{-2}	Maximum braking deceleration
θ	$\in[1/2, 1]$	0.7	Suppression coefficient
$g_{\min_\ell}$	>0 m	$\in$Exp (2/3)	Individual safety clearance

$$x_\ell(t + \mathrm{T}) = x_\ell(t) + \mathrm{T} \cdot v_\ell(t + \mathrm{T}). \tag{49}$$

The outputs of the PLCF model (obtained for the fixed initialization conditions $N = 12$ and $\mathrm{T} = 0.2$, and for a calibrated value of the suppression coefficient θ) are then subjected to standard statistical tests for analyzing a microstructure of the particle ensemble. The results of those tests are plotted in figure 7.

9. Leave-the-intersection models: the annealing-based scheme (AB scheme)

The intention of our article is, *inter alia*, to examine whether the arrangement of vehicles in the vicinity of an intersection is a consequence of traffic rules, complicated evaluation procedures, and sophisticated decision-making procedures or, in contrast, is a consequence of the general stochastic nature of queueing systems. For solving this problem, we intend to create a stochastic alternative for both of the above-discussed models. Thus, we will introduce a unimodal scheme simulating a time evolution of vehicular ensembles without any division into modes (unlike for the GCF model) and without a concept of safe values for some quantities (unlike for the PLCF model).

For these purposes, we have created an original model based on the principles of so-called simulated annealing [42]. We consider N dimensionless particles located along a ring with the circumference equal to N. The initial locations of the particles are generated equidistantly in the interval $[0, N - X]$, where X represents a free gap before the leading vehicle (typically, the distance to the rear of a queue waiting on a previous intersection). The relative velocities $v_\ell(t = 0)$ of all of the vehicles are reset. Then the repeating procedure is applied as follows.

(i) The timing is shifted by 1.
(ii) The quasi-energy of the ensemble is calculated via

$$E(t) = \sum_{\ell=1}^{N-1} \frac{1}{x_\ell(t) - x_{\ell+1}(t)}. \tag{50}$$

(iii) An index $\ell \in \{1, 2, \ldots, N\}$ is picked at random.
(iv) The relative velocity v_ℓ is updated: $v_\ell(t + 1) = \min\{v_\ell(t) + 1/m, 1\}$, where $m \in \mathbb{N}$ is the fixed parameter (see table 8).
(v) Using the formula

$$U_\ell = \frac{\eta}{x_\ell(t) - x_{\ell+1}(t)} + \frac{1}{x_{\ell-1}(t) - x_\ell(t)}, \tag{51}$$

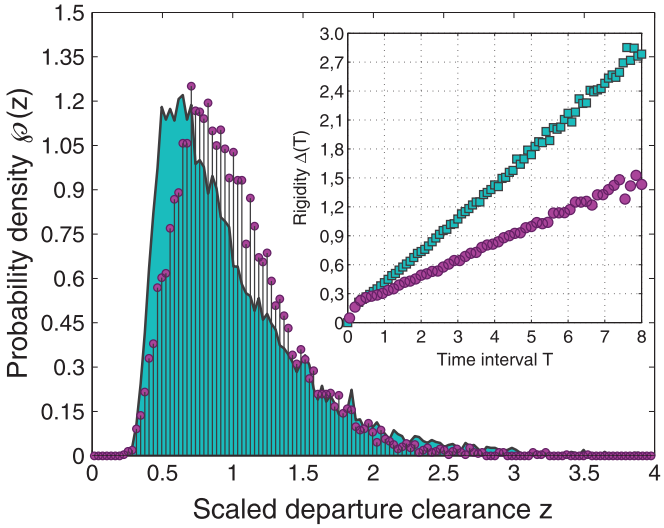

Figure 7. Clearance distributions and statistical rigidities for the PLCF model. The main plot compares the clearance distributions between real-road data (Hradec Králové —circles) and the phenomenological car-following model (the area plot) presented in the text. The comparison between the statistical rigidities (for the same data ensembles) is presented in the inset.

the individual quasi-potential of the ℓth vehicle is calculated. We remark that the coefficient η reduces a influence of the vehicle behind.

(vi) A random number $\delta \backsim \mathrm{Uni}(0,\,1)$ is picked and an anticipated position

$$x_\ell(t+1) = x_\ell(t) + \delta w_{\max}\, v_\ell(t+1) \tag{52}$$

of the ℓth element is computed.

(vii) As the vehicles cannot change their order, we accept $x_\ell(t+1)$ only if $x_\ell(t+1) < x_{\ell-1}(t)$. Moreover, if $x_\ell(t+1) \geqslant x_{\ell-1}(t)$, then the relative velocity should be reduced according to $v_\ell(t+1) := \max\{0,\, v_\ell(t+1) - 1/m\}$.

(viii) The potential

$$U'_\ell = \frac{\eta}{x_\ell(t+1) - x_{\ell+1}(t)} + \frac{1}{x_{\ell-1}(t) - x_\ell(t+1)} \tag{53}$$

of the new configuration is evaluated.

(ix) If $U'_\ell \leqslant U_\ell$, then the position of the ℓth particle takes on a new value: $x_\ell(t+1)$.

(x) If $U'_\ell > U_\ell$, then the Boltzmann factor $\hbar = \exp[-\gamma \Delta U]$, where $\Delta U = U'_\ell - U_\ell$, should be compared with another random number $r \backsim \mathrm{Uni}(0,\,1)$. Provided that the inequality $\hbar > r$ is fulfilled, the position of the ℓth particle takes on the new value $x_\ell(t+1)$ too. Otherwise, the original configuration remains unchanged, i.e. $x_\ell(t+1) = x_\ell(t)$. In this case, the relative velocity is reduced again: $v_\ell(t+1) := \max\{0,\, v_\ell(t+1) - 1/m\}$.

Although the classical scheme of the simulated annealing ensures a relaxation of the ensemble into a thermal equilibrium (see [42]), here we are focused on nonequilibrium states of the above-mentioned particle ensemble. Furthermore, the rules introduced modify the original Metropolis algorithm so dramatically that even if the energy in a system had been established standardly, the proposed scheme would still not lead to a state corresponding to a

Table 8. Parameters of the *AB model*.

Nomenclature	General extent	Option	Description
N	$\in\mathbb{N}$	36	Number of vehicles
m	$\in\mathbb{N}$	10	Number of divisions in the velocity discretization
$w_{\max}$	$\in[2/m, 2]$	0.7	Maximum allowable velocity
γ	$\in[0, +\infty)$	8.15	Randomization parameter
η	$\in[0, 1]$	0.3	Reduction coefficient (reduces the influence of rear gaps)
X	$\in(0, N)$	10.8	Effective distance between intersections
ξ	$(N - X)/(N - 1)$	0.72	Average gap between neighbors in an initial state

classical balance. Those facts are understandable from figure 8, where we investigate the time evolution of the energy (50) in the ensemble. Thus, after 8000 steps (when 15 cars have left the intersection), the system is still significantly far from any equilibrium, which is in consonance with a realistic situation for vehicles.

Five hundred repetitions of that scheme then generated a sufficient amount of inter-vehicle intervals suitable for the intended statistical evaluations. Nonequilibrium distributions of rescaled time gaps in the suggested model (visualized in figure 9) demonstrate illustratively a more significant compliance with real-road statistics than those detected in the previous two models. Similarly, the test of the statistical rigidity (shown in the inset of figure 9) also confirmed that the similarity between the AB model and intersection reality is not accidental.

At this point, it remains to say a few words about a connection of the suggested model with realistic behavior of drivers. Although the model's rules are formulated technically, their background can be interpreted in quite ordinary language. In fact, the AB model is not much more complicated than the model of Nagel and Schreckenberg [43], for example. The main skeleton of the algorithm can be simplified as follows. The car chosen according to a random update procedure tries to accelerate up to maximum velocity (iv) and leap forward by a randomized hopping length (vi). Overtaking is not permitted (vii). Limiting conditions (locations of neighboring cars) are reflected in the force description of the systems. Moreover, the interaction forces/potentials (viii) correspond to an intuitive understanding of vehicular dynamics. As in general physical systems, the ensemble of cars also tends to go predominantly to states with lower potential energy (ix). Nevertheless, since the system investigated is of a stochastic nature, its dynamics allows (with a probability proportional to the level of stochasticity) transitions to states with higher energy (x), similarly to the randomization step in [43].

10. Discussion and concluding remarks

This paper deals with the theoretical and empirical background of vehicular dynamics investigated in the vicinity of signal-controlled intersections. Such a specific area of traffic research exploits the simplicity of inter-vehicle interactions near the traffic lights to obtain a deeper understanding of general laws in vehicular dynamics. Indeed, some complicated traffic phenomena are suppressed there, which provides a unique opportunity for disclosure of the nature of the issue examined.

Since some features of driving behavior are readily predictable (e.g. the middle-ranged nature of mutual interactions), one can formulate certain theoretically substantiated properties of statistical distributions for microscopic vehicular quantities. Using also the well-known

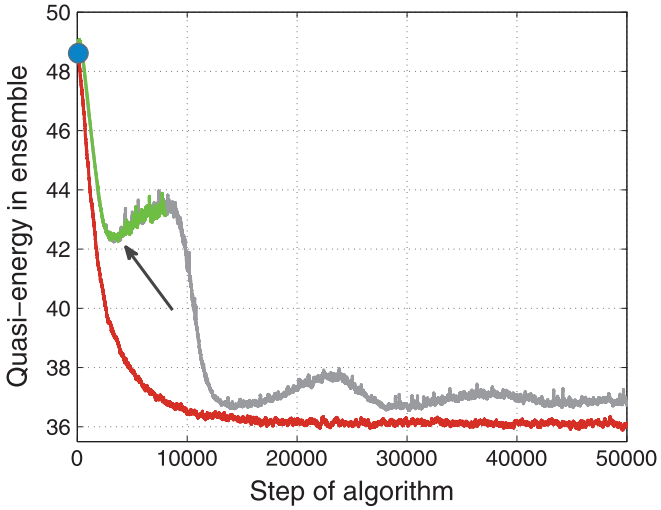

Figure 8. The time evolution of the quasi-energy during the AB algorithm. We plot the average value of the quasi-energy (50) calculated for 500 repeated realizations of the AB algorithm (green curve). For comparison purposes, we also display (see the red curve) the evolution of the energy in a classical variant of the annealing procedure (the so-called *Metropolis algorithm*) simulating a transition of thermal gases into thermodynamical equilibrium. The gray curve demonstrates how the quasi-energy (50) develops if one applies more than 8000 updates. The blue circle represents the initial quasi-energy $E_{\text{ini}} = (N-1)^2/(N-N\xi)$, whereas the gray arrow shows where the leading car has reached the last car waiting at a following intersection.

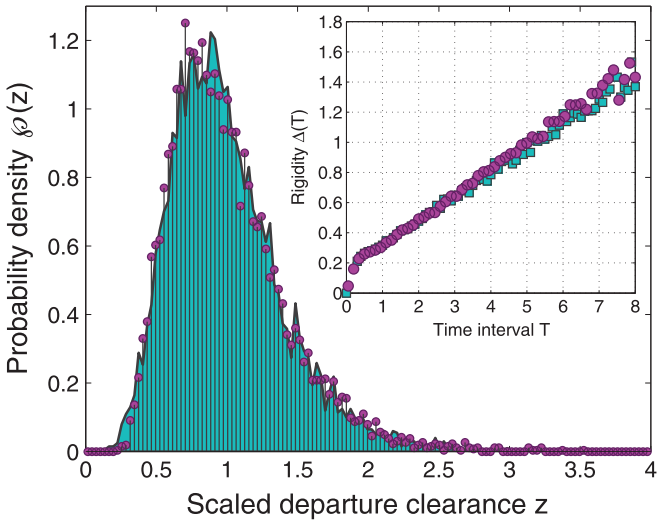

Figure 9. The clearance distribution and statistical rigidity for the AB model. The main plot compares the clearance distributions between Hradec Králové data (red circles) and the annealing-based model (the area plot). The comparison between statistical rigidities (for the same data ensembles) is visualized in the inset.

empirical regularities in the microscopic structure of traffic samples, we have therefore formulated several criteria for the acceptability of mathematical curves proposed for fitting empirical histograms. Sequentially, these criteria can serve to measure the quality of the suggested statistical models. Such evaluations have been tested on several families of distributions in the fourth section. As is evident from these tests, some previously proposed functions are not suitable as estimators for headway statistics. In contrast, the generalized inverse Gaussian distribution (19) (fulfilling all of the acceptance criteria) represents a relevant theoretical prediction for empirical departure–headway statistics. Moreover, these findings have been supported by theoretical and empirical study of the associated statistical rigidities.

The detailed dynamics of vehicles passing the stop line at a signalized intersection has been analyzed by means of three simulation schemes (based on three different approaches). Although all of these microscopic simulators have produced similar departure statistics, the comprehensive analyses (tests of the statistical rigidity) have uncovered some serious discrepancies. The ability to reproduce empirical features of time intervals between two following cars has been confirmed only for the nonequilibrium model based on principles of the simulated annealing. In this case, the consistency between empirical and numerically obtained headways has also been accompanied by a correspondence between the two rigidities.

However, the final outcome of our considerations as regards the origin of the empirical headway distributions is, in fact, extremely surprising. According to our observations, the models with more conspicuous stochastic components (such as the AB scheme) produce more relevant predictions than models stressing certain interaction rules and traffic modes (such as GCF/PLCF schemes). For this reason, it can be speculated that the stochastic component of the system examined dominates the interaction rules as well as the decision-making procedure. Furthermore, it has been demonstrated that the original arrangement of vehicles (before the green signal appears) is stochastically perturbed in an extremely short time. This fact is clearly visible in the AB simulator, where the original equidistant sequencing of vehicles (characterized by a wavy curve of statistical rigidity) is very quickly transformed into the stochastic sequencing (characterized by a linear rigidity significantly distant from the above-mentioned wavy curve). Also the time dependence of the quasi-energy shows the sharpest changes immediately after the beginning of the simulation. All of these facts assure us that the decisive factor for the movement of vehicular ensembles (near the stop line) is the stochasticity.

To conclude, this paper, together with the article [13], gives a comprehensive view of the spatiotemporal course of vehicular ensembles leaving a signalized intersection.

Acknowledgments

The authors would like to thank the students of the Faculty of Nuclear Sciences and Physical Engineering, Czech Technical University, in Prague (attending the seminar $01SMB_2$ on mathematical applications, academic year 2010/2011), and Mr Pavel Křiváň who gauged the traffic data analyzed in this paper. Also, our thanks go to Mr Vít Hanousek who designed an original computer tool suitable for making all the above-discussed measurements. This work was supported by the Czech Technical University within the project SGS12/197/OHK4/3 T/14.

References

[1] Chung K H, Hui P M and Gu G Q 1995 *Phys. Rev.* E **51** 772
[2] Chopard B, Luthi P O and Queloz P A 1996 *J. Phys. A: Math. Gen.* **29** 2325
[3] Brockfeld E, Barlovic R, Schadschneider A3 and Schreckenberg M 2001 *Phys. Rev.* E **64** 056132
[4] Fouladvand M E and Belbasi S 2007 *J. Phys. A: Math. Theor.* **40** 8289
[5] Abdelwahab W M, Ehm R and Mah M 1994 *Canadian Journal of Civil Engineering* **21** 555
[6] Fouladvand M E, Sadjadi Z and Shaebani M R 2004 *J. Phys. A: Math. Gen.* **37** 561
[7] Fouladvand M E, Shaebani M R and Sadjadi Z 2004 *J. Phys. Society Japan* **73** 3209
[8] Ibrahim M R, Karim M R and Kidwai F A 2008 *Am. J. Applied Sci.* **5** 479
[9] Jin X, Zhang Y, Wang F, Li L, Yao D, Su Y and Wei Z 2009 *Transportation Research C: Emerging Technologies* **17** 318
[10] Wang F, Ji Y and Li L 2008 *Int. IEEE Conf. on Intelligent Transportation Systems* p 627
[11] Li L, Wang F, Jiang R, Hu J and Ji Y 2010 *Chinese Phys.* B **19** 020513
[12] Treiber M and Kesting A 2013 *Traffic Flow Dynamics* (Berlin: Springer)
[13] Krbálek M 2008 *J. Phys. A: Math. Theor.* **41** 205004
[14] Chen X, Li L and Zhang Y 2010 *Journal IEEE Transactions on Intelligent Transportation Systems* **11** 773
[15] Helbing D 2001 *Rev. Mod. Phys.* **73** 1067
[16] Kerner B S 2004 *The Physics of Traffic Berlin* (New York: Springer)
[17] Appert-Rolland C 2009 *Phys. Rev.* E **80** 036102
[18] Helbing D, Treiber M and Kesting A 2006 *Physica* A **363** 62
[19] Buckley D J 1968 *Transp. Sci.* **2/2** 107
[20] Chen X Q, Li L, Jiang R and Yang X M 2010 *Chin. Phys. Lett.* **27** 074501
[21] Kerner B S, Klenov S L and Hiller A 2007 *Nonlinear Dyn.* **49** 525
[22] Krbálek M 2010 *Kybernetika* **46** 1108
[23] Tilch B and Helbing D 2000 *Traffic and Granular Flow 99: Social, Traffic, and Granular Dynamics* (Springer) p 333
[24] Krbálek M and Šeba P 2009 *J. Phys. A: Math. Theor.* **42** 345001
[25] Treiber M, Kesting A and Helbing D 2006 *Phys. Rev.* E **74** 016123
[26] Cline D B H and Samorodnitsky G 1994 *Stochastic Processes and their Applications* **49** 75
[27] Teugels J L 1975 *The Annals of Probability* **3** 1000
[28] Krbálek M 2013 *J. Phys. A: Math. Theor.* **46** 445101
[29] Tolle J E 1976 *Transportation Research Record* **567** 56
[30] Luttinen R T 1992 *Transportation Research Record* **1365** 92
[31] Karagiannidis G K, Zogas D A and Kotsopoulos S A 2003 *IEEE Trans. Commun.* **51** 1240
[32] Jørgensen B 1982 Statistical properties of the generalized inverse gaussian distribution (*Lecture Notes in Statistics* vol 9) (New York: Springer) p 188
[33] Krbálek M 2007 *J. Phys. A: Math. Theor.* **40** 581
[34] Krbálek M and Helbing D 2004 *Physica* A **333** 370
[35] Mehta M L 2004 *Random Matrices* 3rd edn (New York: Academic)
[36] Bogomolny E B, Gerland U and Schmit C 2001 *Eur. Phys. J.* B **19** 121
[37] Limpert E, Stahel W A and Abbt M 2001 *Bioscience* **51** 341
[38] Li L, Xiqun C and Zhiheng L 2013 *Transportation Research* F **18** 21
[39] Gazis D C, Herman R and Potts R B 1959 *Oper. Res.* **7** 499
[40] Brackstone M and McDonald M 1999 *Transportation Research Part* F **2** 181
[41] Krauss S 1998 Microscopic modeling of traffic flow: investigation of collision free vehicle dynamics *PhD Thesis* Hauptabteilung Mobilität und Systemtechnik des DLR Köln
[42] Scharf R and Izrailev F M 1990 *J. Phys. A: Math. Gen.* **23** 963
[43] Nagel K and Schreckenberg M 1992 *J. Phys. I France* **2** 2221